Design of Albumin-Coated Microbubbles Loaded With Polylactide Nanoparticles

Marianne Gauthier, PhD, Qian Yin, BS, Jianjun Cheng, PhD, William D. O'Brien Jr, PhD

Objectives—A protocol was designed to produce albumin-coated microbubbles (MBs) loaded with functionalized polylactide (PLA) nanoparticles (NPs) for future drug delivery studies.

Methods—Microbubbles resulted from the sonication of 5% bovine serum albumin and 15% dextrose solution. Functionalized NPs were produced by mixing fluorescent PLA and PLA-polyethylene glycol-carboxylate conjugates. Nanoparticle-loaded MBs resulted from the covalent conjugation of functionalized NPs and MBs. Three NP/MB volume ratios (1/1, 1/10, and 1/100) and unloaded MBs were produced and compared. Statistical evaluations were based on quantitative analysis of 3 parameters at 4 time points (1, 4, 5, and 6 days post MB fabrication): MB diameter using a circle detection routine based on the Hough transform, MB number density using a hemocytometer, and NP-loading yield based on MB counts from fluorescence and light microscopic images. Loading capacity of the albumin-coated MBs was evaluated by fluorescence.

Results—Loaded MB sizes were stable over 6 days after production and were not significantly different from that of time-matched unloaded MBs. Number density evaluation showed that only 1/1 NP/MB volume ratio and unloaded MB number densities were stable over time, and that the 1/1 MB number density evaluated at each time point was not significantly different from that of unloaded MBs. The 1/10 and 1/100 NP/MB volume ratios had unstable number densities that were significantly different from that of unloaded MBs ($P < .05$). Fluorescence evaluation suggested that 1/1 MBs had a higher NP-loading yield than 1/10 and 1/100 MBs. Quantitative loading evaluation suggested that the 1/1 MBs had a loading capacity of 3700 NPs/MB.

Conclusions—A protocol was developed to load albumin MBs with functionalized PLA NPs for further drug delivery studies. The 1/1 NP/MB volume ratio appeared to be the most efficient to produce stable loaded MBs with a loading capacity of 3700 NPs/MB.

Key Words—fluorescence; functionalized nanoparticles; microbubbles; stability

Received March 28, 2014, from the Bioacoustics Research Laboratory, Department of Electrical and Computer Engineering (M.G., W.D.O.), and Department of Materials Science and Engineering (Q.Y., J.C.), University of Illinois at Urbana-Champaign, Urbana, Illinois USA. Revision requested June 9, 2014. Revised manuscript accepted for publication November 19, 2014.

We thank Jamie Kelly and Hua Wang for valuable help with nanoparticle production and fluorescence measurements. This work was supported by National Institutes of Health grant R37EB002641 and Director's New Innovator Award 1DP2OD007246 (to Dr Cheng). This work was presented as part of the New Investigator Award competition at the 2014 American Institute of Ultrasound in Medicine Annual Convention; March 29–April 2, 2014; Las Vegas, Nevada.

Address correspondence to Marianne Gauthier, PhD, Beckman Institute, 4223, University of Illinois at Urbana-Champaign, 405 N Mathews, Urbana, IL 61801 USA.

E-mail: frenchmg@illinois.edu

Abbreviations

BSA, bovine serum albumin; CI, confidence interval; COOH, carboxylate; Cy5, cyanine 5; DMF, dimethylformamide; FITC, fluorescein isothiocyanate; MB, microbubble; PEG, polyethylene glycol; NP, nanoparticle; PLA, polylactide

doi:10.7863/ultra.34.8.1363

Contemporary research has focused on image-guided drug delivery methods and, more specifically, ultrasound-guided drug delivery. The concept of ultrasound-mediated drug delivery was introduced 3 decades ago.[1] Ultrasound-activated drug delivery was developed as a result of the introduction of ultrasound contrast agents: microbubbles (MBs). Their sizes were suitable for purely intravascular circulation, and they consisted of a gaseous core stabilized by a shell composed of lipids, proteins, or polymers. In response to an ultrasonic pressure wave, MBs expand and collapse, facilitating the intravascular delivery of injected drugs

to tissue.[2] However, this approach based on the coinjection of freely circulating drugs and MBs followed by the local application of ultrasound has raised toxicity, solubility, and clearance issues related to regular systemic drug delivery of highly toxic chemotherapeutics.[3,4] To address these issues and increase payload delivery, drug-loaded MBs have been developed: MBs have been developed as vehicles loaded with a therapeutic agent, identified at the target site via imaging, and then collapsed using high-amplitude ultrasonic pulses to release the therapeutic agent locally. However, with such formulations, drug-loaded MBs face major challenges: first, MBs have short circulation times in vivo, and second, MBs have poor loading capacities.[5,6] Both challenges yield an inefficient therapeutic delivery vehicle.[7–10] To address the poor loading limitation, nanoparticle (NP)-loaded MBs have been studied,[8,11–13] as they theoretically possess the drug delivery payload capacity of NPs combined with the echogenicity of the MBs. One strategy to attach the NP to the MB surface involves covalent linking.

In this study, carbomiide was used to covalently link functionalized polylactide NPs with albumin-coated MBs to produce NP-loaded MBs. The study's objective was to compare 3 formulations to determine an efficient protocol to produce stable NP-loaded MBs for future drug delivery purposes.

Materials and Methods

Production of NP-Loaded MBs

Microbubbles (final number density of $3.6 \pm 0.104 \times 10^8$ MBs/mL) were produced by mixing 1.5 mL of 5% bovine serum albumin (BSA; Sigma-Aldrich Co, St Louis, MO) and 4.5 mL of 15% dextrose (Fisher Chemical, Fair Lawn, NJ).[14] The resulting solution was then vortexed, saturated with perfluorobutane gas (FluoroMed, LP, Round Rock, TX), and sonicated for a duration of 70 seconds at 250 W with a 20-kHz Fisher 500 sonic dismembrator (Thermo Fisher Scientific, Waltham, MA). The unloaded MB mean concentration and diameter were determined to be 3.6×10^8 MB/mL and 0.77 μm, respectively.

As fully described,[15] cyanine 5 (Cy5)-PLA conjugates were produced by first adding beta-diimine-zinc nitride $(\text{tetramethylsilane})_2$ catalysts (7.0 mg, 0.01 mmol) to a Cy5 solution made by dissolving Cy5 (2.5 mg, 0.005 mmol) in 1 mL of anhydrous tetrahydrofuran. Lactide (TCI America, Portland, OR; 72 mg, 0.5 mmol) was added dropwise to the Cy5 solution, and the resulting Cy5-PLA conjugates (100 μL of dimethylformamide [DMF], 10 mg/mL) were polymerized in the presence of PLA-monomethoxy polyethylene glycol (PEG; Sigma-Aldrich Co; 100 μL of DMF, 10 mg/mL) to produce the Cy5-PLA–conjugated NPs. Briefly, a DMF solution of the Cy5-PLA conjugate (200 μL, 20 mg/mL) and polylactide-PEG-carboxylate (COOH) conjugate (200 μL, 20 mg/mL) was mixed and added dropwise to nanopure water (8 mL). The resulting NP suspension was purified by ultrafiltration (5 minutes, 3000g; Ultracel membrane with a 10,000 nominal molecular weight limit; Millipore, Billerica, MA) and washed with water. The Cy5-functionalized NP final concentration was 5 mg/mL. Additional quantitative evaluation was performed using PLA NP-loaded MBs labeled with fluorescein isothiocyanate (FITC) for laboratory considerations. Briefly, 3 polymer solutions were prepared by mixing solid polymers [poly(DL-lactide)-fluorescein, poly(DL-lactide)-b-PEG-carboxylic acid, and methoxy-PEG-b-poly(DL) lactic acid; Akina Inc, West Lafayette, IN) with DMF to produce 10 mg polymer/mL DMF solutions; 0.167 mL of each polymer solution was mixed via pipetting in a glass vial and added dropwise to 10 mL of deionized water stirred at 200 revolutions per minute via a stir bar. After 5 minutes, the solution was transferred to a 10,000 molecular weight cutoff centrifuge filter tube and spun at 2500 revolutions per minute for 15 minutes to bring the final volume to 1 mL for FITC-NP solution with a final concentration of 5 mg of NP/mL.

Nanoparticle functionalization was performed by mixing the previous Cy5 and FITC-NP solutions with 60 μL of 1-(3-dimethylaminopropyl)-3-ethylcarbodiimide hydrochloride (310 mg/mL) and 60 μL of N-hydroxysuccinimide (28.3 mg/mL).[15] The resulting activated NPs were allowed to react for several hours with the MBs: functionalized NP-COOH groups reacted to N-hydroxysuccinimide in the presence of 1-(3-dimethylaminopropyl) -3-ethylcarbodimide hydrochloride, resulting in an N-hydroxysuccinimide ester, which then reacted with primary amine (-NH2) from MB albumin. Buoyancy separation was used to remove the excess NPs after several washes using phosphate-buffered saline (Sigma-Aldrich Co).

Nanoparticle/MB volume ratios are defined in terms of the volume of the NP solution added to the MB solution, knowing that the NP mass concentration and the MB number density are 5 mg/mL and 3.58 × 108 MBs/mL, respectively. The NP/MB volume ratios are denoted herein as ratios 1/1, 1/10, and 1/100. The reaction is illustrated in Figure 1.

Four groups have been evaluated. Based on preliminary observations, 3 NP/MB volume ratios were tested: 1/1 volume ratio (Cy5-functionalized NP: 1 mL/MB: 1 mL),

1/10 volume ratio (Cy5-functionalized NP: 0.1 mL/MB: 1 mL), and 1/100 volume ratio (Cy5-functionalized NP: 0.01 mL/MB: 1 mL). In addition, a separate batch of unloaded MBs was monitored as reference for the analysis. The NP-loaded MB and unloaded MB diameter and number density as well as NP-loading yield were determined at 4 time points (days 1, 4, 5, and 6 after MB production) as described below.

Size Evaluation

The size evaluation method used herein has already been described.[16] Briefly, to estimate MB size, 10 images of the MB solution were acquired using a microscope (BX51; Olympus Optical, Tokyo, Japan) with a resolution of 0.06 μm/pixel. On hundred MBs were randomly selected from the microscopic acquisitions and analyzed using a MATLAB-coded (The MathWorks, Natick, MA) circular-shaped detection routine based on the Hough transform.[17] The mean diameter and its 95% confidence interval (CI) were calculated for each volume ratio at each time point.

Number Density Evaluation

The MB number density (MBs/mL) was evaluated using a hemocytometer (Hausser Scientific, Buffalo, NY). At each time point, NP-loaded MB and unloaded MB solutions were sampled and diluted with phosphate-buffered saline (10%, vol/vol). Hemocytometer chambers were filled with 10 μL of the diluted MB solution and imaged at ×20 magnification (Olympus BX51). Four MB counts were realized from a 1 × 1-mm area from which the mean number density was calculated along with its 95% CI for each volume ratio at each time point.

Nanoparticle-Loading Yield Evaluation

Functionalized NPs were labeled with Cy5, a cyanine used as a dye and soluble in water, which exhibits absorption and emission wavelengths of 649 and 670 nm, respectively. To evaluate the NP-loading yield for the different NP/MB volume ratios, the NP-loaded MB solution was sampled and imaged using light microscopy followed by fluorescence microscopy. Images of the same slide region were acquired using an Axiovert 40CFL inverted microscope (Carl Zeiss Meditec, Inc, Dublin, CA), saved, and processed using ImageJ (National Institutes of Health, Bethesda, MD). Images were converted to black and white and adjusted using the Threshold tool. The Analyze Particle tool was thus used to provide the count of the MBs. Light microscopy provided the MB number density associated with NP-loaded MBs and unloaded MBs, as both types of MBs were imaged. The fluorescence imaged only the MBs tagged with NPs (NP-loaded MPs) because fluorescence was associated with the Cy5-tagged NPs. Consequently, the resulting count from images acquired using light microscopy was the total MB number density (NP-loaded + unloaded; Figure 2A), whereas the count associated with the fluorescence image was the NP-loaded MB number density (Figure 2B). The NP-loading yield, defined as the NP-loaded MB number density divided by the total MB number density, was then determined and analyzed. Three counts were performed by 2 operators at each time point for each volume ratio to provide the 95% CI for each mean NP-loading yield percentage.

Statistical Evaluation

Size, number density, and NP-loading yield statistical analyses were performed by means of the statistical envi-

Figure 1. Schematic representation of the covalent linking of PLA NPs to the albumin MB shell via the carbodiimide technique: NPs are loaded to the MB shell through an amine bond between the carboxyl groups on the NP surface and the amine groups on the MB surface. EDC indicates 1-(3-dimethylaminopropyl)-3-ethylcarbodiimide hydrochloride; and NHS, *N*-hydroxysuccinimide.

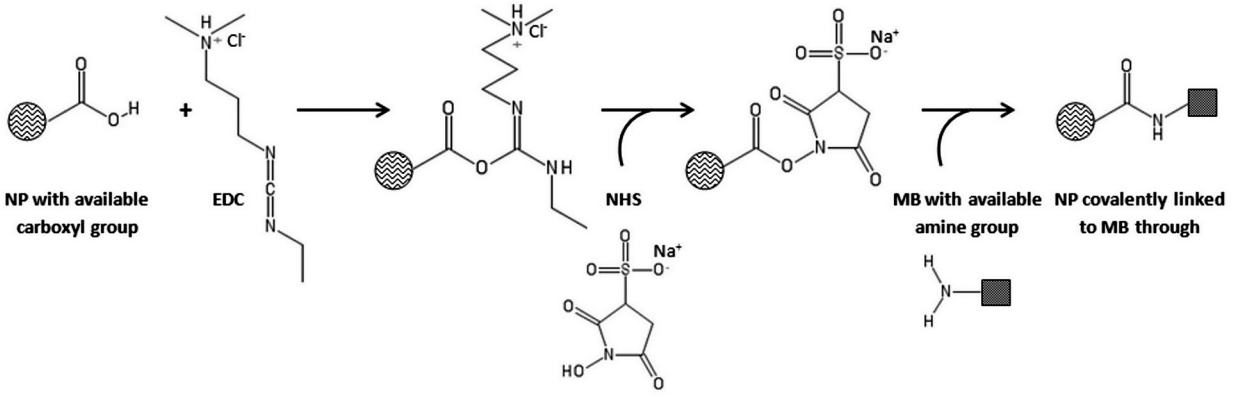

ronment R (version 3.0.2; R Foundation for Statistical Computing, Vienna, Austria; open access available at: http://cran.r-project. org). Size, number density, and NP-loading yield evaluations were based on comparing the parameters between and within the groups. Results were significant at $P < .05$.

Between-Group Comparison

Normality of distributions for each time point and equality of variances between time-matched values were tested using, respectively, Shapiro and *F* tests before any further analyses. For normal distributions with equality of variances, comparison between time-matched parameters was performed using a Welch *t* test. Otherwise, comparison between time-matched parameters was performed using a nonparametric Wilcoxon test that did not require any assumption concerning neither the condition of normality nor the equality of variances.

Within-Group Comparison

Normality of the distributions over the 4 time points and equality of variances for the distributions were tested using, respectively, Shapiro and Levene tests before any further analyses. For normal distributions, within-group analysis was performed using a 1-way analysis of variance. For significant results, post hoc analysis was run using the Tukey test with Bonferronni adjustment to determine which groups were different from the others. For non-normal distributions, a nonparametric Kruskal-Wallis test was run and completed by a post hoc multiple comparison with Bonferronni adjustment when results from Kruskal-Wallis analysis were significant.

Gas-Filled NP-Loaded MBs

Double passive cavitation detection is a validated method[17–19] for determining cavitation characteristics including collapse thresholds of isolated MBs based on the detection of a postexcitation signal occurring 1 to 5 microseconds after the principle excitation of the bubble.

Integrity of the gas-filled MBs loaded with the NPs for the 1/1 NP/MB volume ratio has been tested using double passive cavitation detection. Briefly, the double passive cavitation detection experiments involved a 4.6-MHz transmit transducer and 13.8- and 14.6-MHz receive transducers. Three-cycle tone bursts at the center frequency of the transmit transducer with a pulse repetition frequency of 10 Hz were generated using a pulse receiver system (RAM500; RITEC, Warwick, RI). Several thousand signals (21 series of 500 signals) were acquired. The complete setup, including the transmit peak rarefactional pressure amplitude calibration as well as the signal classification, has been fully described.[19] The measurement criterion in this study was the postexcitation threshold percentage, defined as the level at which a certain percentage of the total population of MBs transiently collapses with the postexcitation signal for an applied peak rarefactional pressure amplitude. Postexcitation curves were then obtained using a modified logistic regression in MATLAB to fit the experimental data, allowing the evaluation of the 5% and 50% postexcitation thresholds and their 95% CIs.[19]

Loading Capacity of the Albumin-Coated MBs

Additional loading capacity analyses were performed on NP-loaded MBs labeled with FITC. The FITC fluorescence standard curve was measured at an excitation wavelength of 495 nm to determine the emission wavelength associated with the maximum fluorescence intensity.

Figure 2. ImageJ-processed light microscopic image (**A**) and fluorescence microscopic image (**B**). Edges of the elements detected in both images were provided by ImageJ to allow the determination of number density.

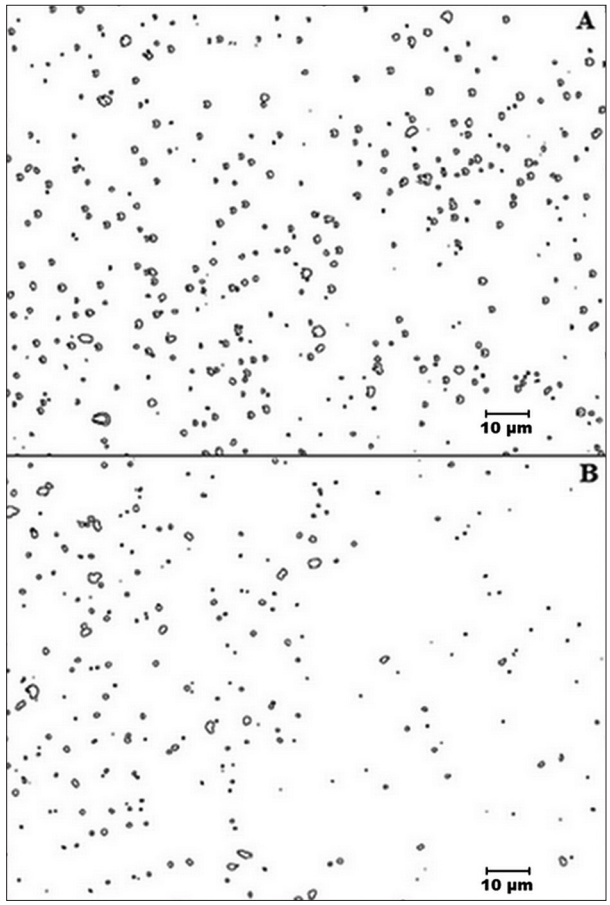

Thus, intensity values at the determined emission wavelength were measured for several FITC concentrations to draw the standard intensity/concentration curve and set its associated equation from which the true FITC concentrations of the NP and NP-loaded MBs solutions were determined. Evaluating the amount of NPs per MB was based on the assumption that the NPs were spherical in shape and had a polymeric solid core. Also, PEG and PLA densities were assumed to be, respectively, 1.13 and 1.09 g/cm^3,[20] leading to the assumption of a density of 1.0 g/cm^3 for the NPs. Last, NP size was estimated using a dynamic light-scattering method (15-mW laser; incident beam = 676 nm; Brookhaven Instruments, Holtsville, NY).

Results

Size Evaluation (Figure 3)

Between-Group Comparison (Table 1)

At each time point, NP-loaded MB (volume ratios 1/1, 1/10, and 1/100) and unloaded MB size variances were significantly different. In addition, distributions did not meet the normality condition. The 1/1 NP-loaded MB sizes were not significantly different from that of time-matched unloaded MBs. On the other hand, 1/10 and 1/100 NP-loaded MB sizes had significantly different time-matched size values, respectively, at days 1 and 5.

Within-Group Comparison (Table 2)

Nanoparticle-loaded MB (volume ratios 1/1, 1/10, and 1/100) and unloaded MB size variances were not significantly different within the groups. However, the normality condition was not satisfied. The 1/1 and 1/10 NP-loaded MB and unloaded MB sizes did not show significant differences over time. Significant differences were found for 1/100 NP-loaded MBs: MB size evaluated at day 5 was significantly different from that at days 1 and 4, as suggested by the post hoc analysis (Table 3).

Figure 3. Nanoparticle-loaded MB (volume ratios 1/1, 1/10, and 1/100) and unloaded MB (uMB) mean diameter as a function of time. Error bars represent the 95% CIs. D indicates day.

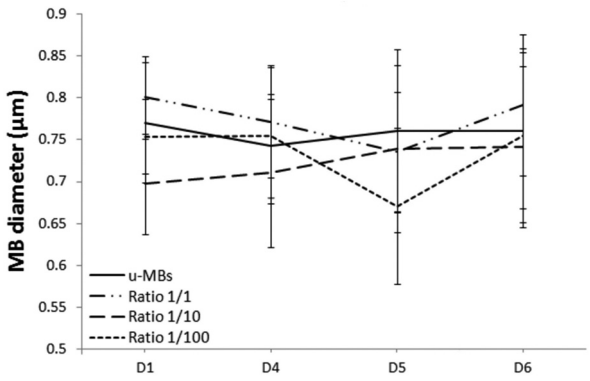

Number Density Evaluation (Figure 4)

Between-Group Comparison (Table 1)

Overall, loaded and unloaded MB time-matched number density variances were significantly different. However, the normality condition was verified for each group at each time point. Between group analysis suggested that only 1/1 NP-loaded MB number density values were not significantly different from that of time-matched unloaded MBs.

Within-Group Comparison (Table 2)

Nanoparticle-loaded MB (volume ratios 1/1, 1/10, and 1/100) and unloaded MB number density variances were not significantly different within the groups, and the normality condition was satisfied for each group. The 1/1 NP-loaded MB and unloaded MB number density values did not show significant differences over time, whereas significant results

Table 1. *P* Values for the Between-Group Analyses Performed at Each Time Point Between 1/1, 1/10, and 1/100 MBs and Time-Matched Unloaded MBs for Size and Number density and Between 1/10 and 1/100 MBs and Time-Matched 1/1 MBs for NP-Loading Yield

Evaluation	Day	1/1	1/10	1/100
Size	1	.20	.02[a]	.89
(vs time-matched	4	.47	<.008[a]	.56
unloaded MBs)	5	.09	.27[a]	<.001[a]
	6	.13	.42[a]	.27
Number density	1	.21	<.001[a]	.15
(vs time-matched	4	.10	<.001[a]	.24
unloaded MBs)	5	.19	<.01[a]	.45
	6	.11	<.001[a]	.001[a]
NP-loading yield	1		.14	.03[a]
(vs time-matched 1/1 MBs)	4		<.001[a]	<.001[a]
	5		<.01[a]	<.01[a]
	6		<.001[a]	<.001[a]

[a]Significant results.

Table 2. *P* values for the Within-Group Analyses Performed for Size, Number Density, and NP-Loading Yield Over the 4 Time Points for NP-Loaded MBs (NP/MB volume ratios) and Unloaded MBs

Evaluation	Unloaded	1/1	1/10	1/100
Size	.12	.10	.72	<.001[a]
Number density	.09	.18	<.001[a]	<.01[a]
NP-loading yield		.04[a]	.04[a]	.02[aa]

[a]Significant results.

were found for 1/10 and 1/100 NP-loaded MBs. Post hoc analyses (Table 3) suggested that significant differences for 1/10 and 1/100 NP-loaded MB number density values, respectively, came from days 4 and 6.

Nanoparticle-Loading Yield Evaluation (Figure 5)

Between-Group Comparison (Table 1)

Overall, time-matched NP-loading yield variances differed. However, the normality condition was satisfied for each group. Between-group analysis suggested that 1/1 NP-loaded MB loading yields were significantly different from time-matched 1/10 and 1/100 NP-loaded MBs.

Within-Group Comparison (Table 2)

Nanoparticle-loaded MB (volume ratios 1/1, 1/10, and 1/100) NP-loading yield variances were not significantly different within the groups. However, the normality condition was not valid when the whole population was taken into account. Within-group analysis suggested that all NP-loaded MB groups showed significantly different NP-loading yields over time. Post hoc analyses (Table 3) suggested that 1/10 and 1/100 NP-loading yields decreased significantly from day 1, whereas 1/1 loading yields were not significantly different over the first 5 days.

Gas-Filled NP-Loaded MBs (Figure 6)

Double passive cavitation detection experiments were performed for 1/1 NP-loaded MBs at day 4. Results suggested that the 50% postexcitation threshold was a 5.3-MPa peak rarefactional pressure amplitude (5.14–5.50), which was in agreement with previous findings on commercially available MBs.[19] The possibility of detecting the collapse threshold for the NP-loaded MBs suggested that MBs were still acoustically active and might be used for future in vivo experiments.

Loading Capacity of the Albumin-Coated MBs

Figure 7A shows the FITC fluorescence standard curve for an excitation wavelength of 495 nm: the maximum fluorescence intensity was found for a wavelength of 517 nm. Consequently, FITC intensity values were measured at 517 nm for several FITC concentrations, yielding an FITC

Table 3. *P* Values for the Post Hoc Tests Performed After the Between-Group Analyses for Size, Number Density, and NP-Loading Yield for Each Significant NP/MB Volume Ratio

	Size	Number Density		NP-Loading Yield		
Days	1/100	1/10	1/100	1/1	1/10	1/100
1–4	.50	.002	.91	>.99	.35	.08
1–5	<.001[a]	.89	.99	.33	.03[a]	.004
1–6	<.005[a]	.40	.02[a]	.01[a]	.008	<.001[a]
4–5	<.001[a]	<.001[a]	.97	>.99	.89	.35
4–6	.52	.04[a]	.007[a]	.06	.19	.004[a]
5–6	.061	.13	.02[a]	.33	>.99	.08

[a]Significant results.

Figure 4. Nanoparticle-loaded MB (NP/MB volume ratios 1/1, 1/10, and 1/100) and unloaded MB (uMB) mean number density as a function of time. Error bars represent the 95% CIs. D indicates day.

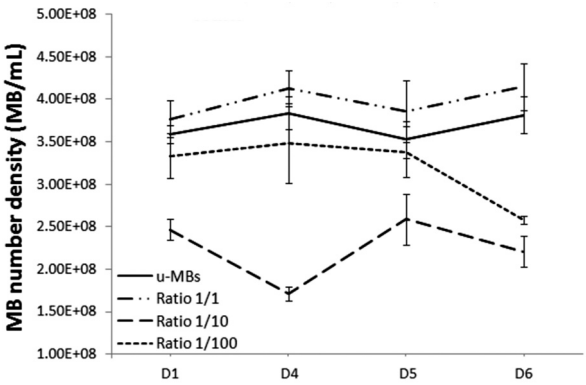

Figure 5. Nanoparticle-loaded MB (NP/MB volume ratios 1/1, 1/10, and 1/100) NP-loading yield as a function of time. Error bars represent 95% CIs; 100% corresponds to the total number of MBs detected that showed fluorescence. D indicates day.

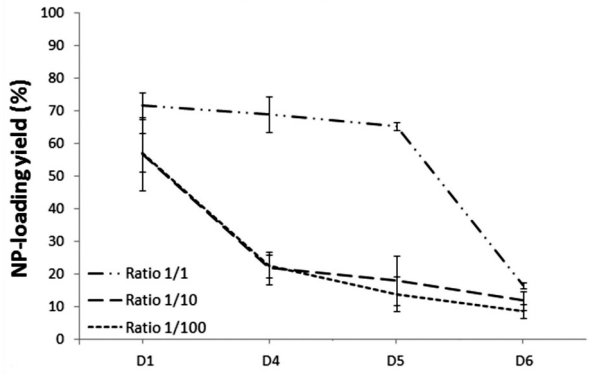

intensity/concentration standard curve described by the following regression equation (Figure 7B): fluorescence intensity = 8.55 × FITC concentration + 23.16.

Our evaluations suggested FITC concentrations for NP and NP-loaded MB solutions of 4533 and 771 ng/mL, respectively. Considering an initial MB number density of 3.6×10^8 MBs/mL and an initial NP solution of 5 mg/mL, the mass of NPs loaded per MB was evaluated to be 6.5×10^{-9} mg NP/MB. Last, dynamic light scattering suggested a mean NP size of 130 nm. Thus, based on both measurements performed and assumptions, the analysis suggested that the loading capacity of the MB was 3700 NPs/MB.

Figure 6. Postexcitation percentage curve for 1/1 NP-loaded MBs plotted against peak rarefactional pressure amplitude (PRPA) at 4.6 MHz. The solid curve represents the logistic fit, and the dashed curves represent the 95% CIs.

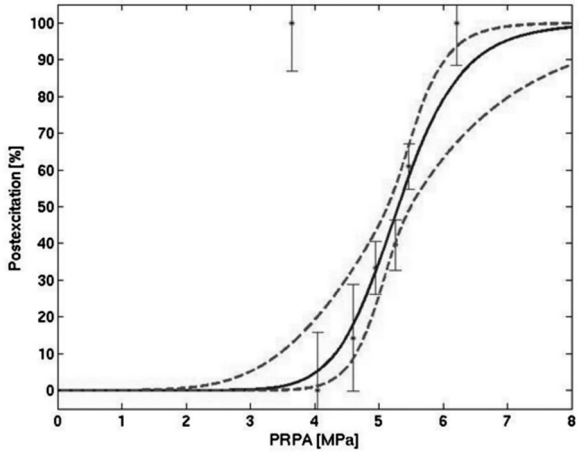

Discussion

Several approaches have been studied to attach NPs to MB surfaces, involving either avidin-biotin interactions[5,21–27] or covalent binding.[28–31] As avidin-biotin NP-loaded MBs cannot be transferred to clinical use because repeated injections may induce an adverse immune response, we decided to produce NP-loaded MBs using carbomiide to covalently link functionalized Cy5-PLA NPs to albumin-coated MBs. To our knowledge, few studies have focused on developing NP-loaded albumin MBs,[12,32] and none have been found in the literature mentioning PLA NP-loaded albumin-coated MBs.

In this contribution, we developed a protocol to load NPs onto the MB surface to increase payload capacity. We compared NP-loaded MBs produced using the same protocol but involving 3 NP/MB volume ratios.[12,13] The NP/MB volume ratios are defined in terms of the volume of the NP solution added to the MB solution, knowing the NP mass concentration and the MB number density. The NP/MB volume ratio (denoted herein as ratios 1/1, 1/10, and 1/100) is only a rough, qualitative intent to understand the stability issues as a function of the number of NPs that are attached to MBs. Previous work had established that 1-μm unloaded MBs, identical to those prepared herein, were stable over several weeks when stored at room temperature.[33] Our study demonstrated that the NP-loaded MB volume ratios showed temporal stability in size and number density for at least a 5-day duration relative to those of the time-matched unloaded MBs. However, fluorescence analysis showed significant differences between the NP-loading yields after a 1-day duration.

Figure 7. **A**, Fluorescence spectra of FITC with an excitation wavelength of 495 nm: the maximum emission wavelength was found at 517 nm. **B**, FITC standard curve: fluorescence intensity values at 517 nm as a function of FITC concentration.

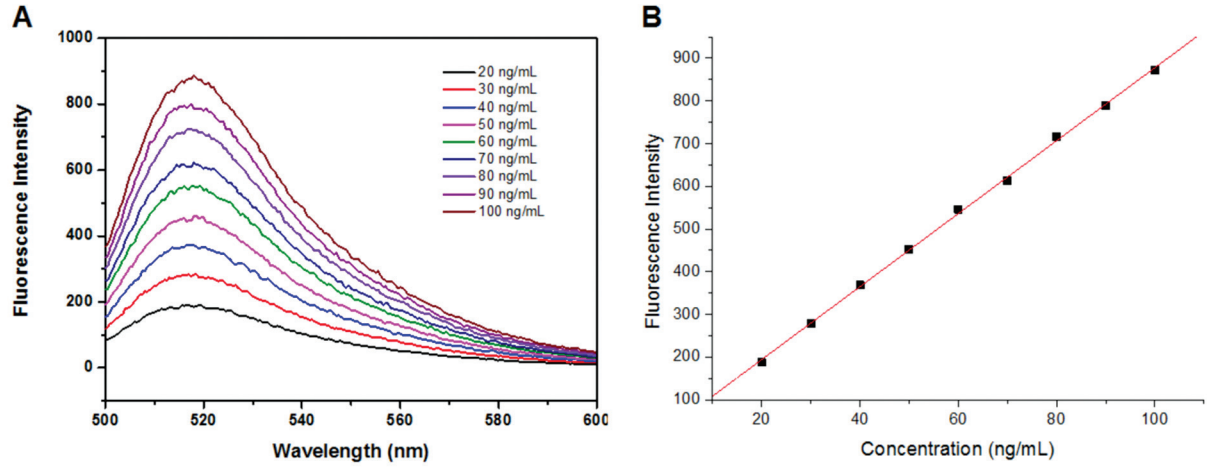

The MBs loaded with the highest NP payload had a temporally stable fluorescence yield of about 70% for at least a 5-day duration, whereas the MBs loaded with the 2 smaller payloads had significantly decreased yields to about 10% after a 1-day duration.

Such a detected decrease in NP-loading yield might be related to the fluorescence evaluation method, which was limited by the sensitivity of the fluorescence. Indeed, the technique used herein followed Boolean logic: MBs were either fluorescent or not. Consequently, it is most likely that the decreasing amount of NPs became too low to be detected and reported as NP-loaded MBs in the fluorescence evaluation for 1/10 and 1/100, resulting in a much lower NP-loading yield than that of 1/1. Although this study demonstrated that the 1/1 NP/MB volume ratio undeniably produced NP-loaded MBs with a higher stable NP-loading yield than 1/10 and 1/100, a method to truly quantify the amount of attached NPs might be required for future studies.

For all NP/MB volume ratios, loading issues may have occurred. In particular, NPs may have interacted with the freely circulating BSA remaining from the sonication process, resulting in the production of fluorescent particles that were not NP-loaded MBs. In the future, the excess of BSA might be removed using centrifugal flotation, filtration, or buoyancy of MBs.

In addition, although albumin-coated MBs are generally stable for several years in the aqueous phase under refrigerated storage conditions, the newly designed NP-loaded MBs showed stability over a 5-day duration, thus questioning their practical clinical use but nonetheless demonstrating clinical potential. We recently focused on the 1/1 NP/MB volume ratio protocol and conducted a longer stability study on NP-loaded MBs tagged with FITC. Our current results suggest an increased stability of at least 1-month duration with a loading capacity of around 95%. This improved stability is likely related to improved skills in producing the 1/1 NP-loaded MBs.

Currently, our MB fabrication procedures use BSA for practical and laboratory safety considerations. However, BSA would trigger an immunogenic response when injecting in humans. The translational aspect of this study is based on the possibility of applying the same protocol to produce MBs using human serum albumin, as previously described.

Loading drugs in the current NPs has yet to be investigated and fully characterized. However, under an Institutional Animal Care and Use Committee–approved protocol, we recently tested the 1/1 NP/MB protocol in vivo to produce NP-loaded MBs labeled with FITC by comparing the fluorescent uptake in 4T1 tumors after NP-loaded MBs or NPs only were injected into BALB/c mice. The tumor region was then imaged with ultrasound at a high mechanical index to collapse the MBs. We demonstrated that while undergoing high–mechanical index ultrasound imaging, NP-loaded MBs showed a higher NP release into the tumor than NPs only (Figure 8): attaching NPs at the MB surface improved the local release of the NPs in tumors, thus opening the way for future drug delivery techniques.

Last, the study suggested that the loading capacity of the albumin-coated MBs for the 1/1 MBs was 3700 NPs/MB. These results are in agreement with previous studies,[8,11,13,34] thus confirming the possible use of the newly

Figure 8. Left (**A**) and right (**B**) 4T1 tumor tissue sections from a BALB/c mouse incubated with collagen IV and Cy5-labeled donkey anti-rabbit immunoglobulin G. Tumor sections were imaged at ×200 using FITC, 4′,6-diamidino-2-phenylindole, and Cy5 filters.

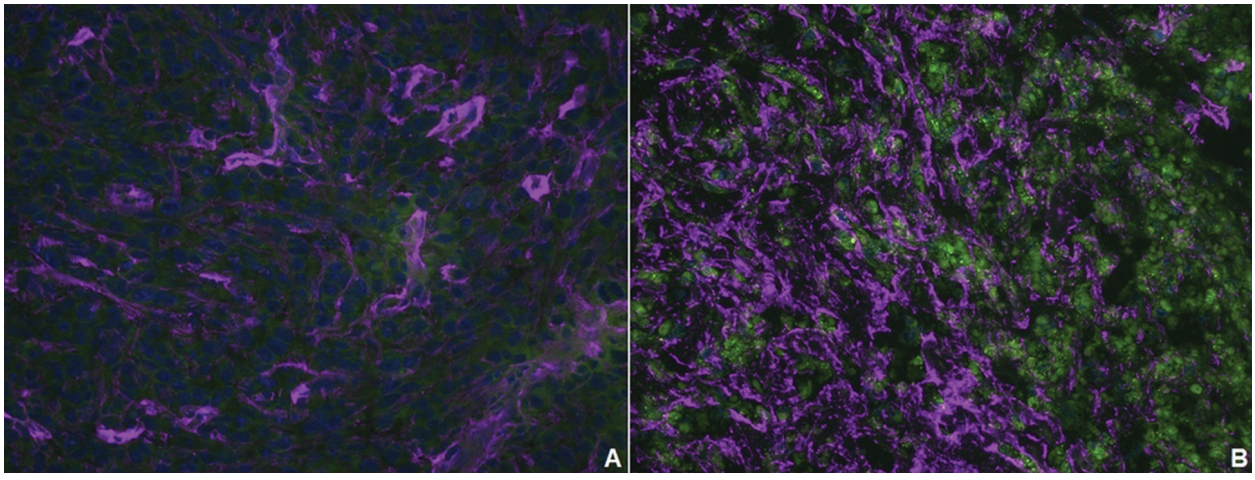

designed NP-loaded MBs for further drug delivery studies.

In conclusion, overall, MBs loaded with the highest payload showed temporally stable physical parameters that were similar to those of unloaded MBs as well as showing longer and stronger fluorescence. The greater temporal stability makes available the possibility for additional research opportunities, such as not needing to fabricate the NP-loaded MBs on site for immediate use or for fabricating a larger number of NP-loaded MBs when needed on a single experiment day. Continued protocol improvements are needed for NP-loaded MBs to have comparable stability to those of unloaded MBs. This contribution has demonstrated a proof of concept; more work is of course required for NP-loaded MBs to become a viable product.

References

1. Miyazaki S, Hou WM, Takada M. Controlled drug release by ultrasound irradiation. *Chem Pharm Bull (Tokyo)* 1985; 33:428–431.
2. Ward M, Wu J, Chiu JF. Ultrasound-induced cell lysis and sonoporation enhanced by contrast agents. *J Acoust Soc Am* 1999; 105:2951–2957.
3. Chen Y, Jungsuwadee P, Vore M, Butterfield DA, St Clair DK. Collateral damage in cancer chemotherapy: oxidative stress in nontargeted tissues. *Mol Interv* 2007; 7:147–156.
4. Carvalho C, Santos RX, Cardoso S, et al. Doxorubicin: the good, the bad and the ugly effect. *Curr Med Chem* 2009; 16:3267–3285.
5. Willmann JK, Cheng Z, Davis C, et al. Targeted microbubbles for imaging tumor angiogenesis: assessment of whole-body biodistribution with dynamic micro-PET in mice. *Radiology* 2008; 249:212–219.
6. Hernot S, Klibanov AL. Microbubbles in ultrasound-triggered drug and gene delivery. *Adv Drug Deliv Rev* 2008; 60:1153–1166.
7. Li P, Zheng Y, Ran H, et al. Ultrasound triggered drug release from 10-hydroxycamptothecin-loaded phospholipid microbubbles for targeted tumor therapy in mice. *J Control Release* 2012; 162:349–354.
8. Geers B, Lentacker I, Sanders NN, Demeester J, Meairs S, De Smedt SC. Self-assembled liposome-loaded microbubbles: the missing link for safe and efficient ultrasound triggered drug-delivery. *J Control Release* 2011; 152:249–256.
9. Cochran MC, Eisenbrey J, Ouma RO, Soulen M, Wheatley MA. Doxorubicin and paclitaxel loaded microbubbles for ultrasound triggered drug delivery. *Int J Pharm* 2011; 414:161–170.
10. Rapoport N, Nam KH, Gupta R, et al. Ultrasound-mediated tumor imaging and nanotherapy using drug loaded, block copolymer stabilized perfluorocarbon nanoemulsions. *J Control Release* 2011; 153:4–15.
11. Klibanov AL, Shevchenko TI, Raju BI, Seip R, Chin CT. Ultrasound-triggered release of materials entrapped in microbubble-liposome constructs: a tool for targeted drug delivery. *J Control Release* 2010; 148:13–17.
12. Gauthier M, Yin Q, Cheng J, O'Brien WD Jr. Production of albumin-coated microbubbles loaded with polylactide nanoparticles [abstract]. *J Ultrasound Med* 2014; 33(suppl):S38.
13. Kheirolomoom A, Dayton PA, Lum AF, et al Acoustically-active microbubbles conjugated to liposomes: characterization of a proposed drug delivery vehicle. *J Control Release* 2007; 118:275–284.
14. Borrelli MJ, O'Brien WD Jr, Bernock LJ, et al. Production of uniformly sized serum albumin and dextrose microbubbles. *Ultrason Sonochem* 2012; 19:198–208.
15. Tong R, Coyle VJ, Tang L, Barger AM, Fan TM, Cheng J. Polylactide nanoparticles containing stably incorporated cyanine dyes for in vitro and in vivo imaging applications. *Microsc Res Tech* 2010; 73:901–909.
16. Gauthier M, Yin Q, Cheng J, O'Brien WD Jr. Production approaches for microbubbles loaded with nanoparticles. In: *Proceedings of the 2013 Joint UFFC, EFTF, and PFM Symposium*. Piscataway, NJ: Institute of Electrical and Electronics Engineers; 2013:1521–1524.
17. King D, O'Brien WD Jr. Quantitative analysis of ultrasound contrast agent postexcitation collapse [correspondence]. *IEEE Trans Ultrason Ferroelectr Freq Control* 2013; 61:1237-41.
18. Gauthier M, King D, O'Brien W. Influence of microbubble size on postexcitation collapse thresholds for single ultrasound contrast agents using double passive cavitation detection. *IEEE Trans Ultrason Ferroelectr Freq Control* 2013; 60:877–879.
19. King DA, Malloy MJ, Roberts AC, Haak A, Yoder CC, O'Brien WD Jr. Determination of postexcitation thresholds for single ultrasound contrast agent microbubbles using double passive cavitation detection. *J Acoust Soc Am* 2010; 127:3449–3455.
20. Ahmed F, Discher DE. Self-porating polymersomes of PEG-PLA and PEG-PCL: hydrolysis-triggered controlled release vesicles. *J Control Release* 2004; 96:37–53.
21. Ellegala DB, Leong-Poi H, Carpenter JE, et al. Imaging tumor angiogenesis with contrast ultrasound and microbubbles targeted to alpha(v)beta3. *Circulation* 2003; 108:336–341.
22. Leong-Poi H, Christiansen J, Klibanov AL, Kaul S, Lindner JR. Noninvasive assessment of angiogenesis by ultrasound and microbubbles targeted to alpha(v)-integrins. *Circulation* 2003; 107:455–460.
23. Ottoboni S, Short RE, Kerby MB, Tickner EG, Steadman E, Ottoboni TB. Characterization of the in vitro adherence behavior of ultrasound responsive double-shelled microspheres targeted to cellular adhesion molecules. *Contrast Media Mol Imaging* 2006; 1:279–290.
24. Takalkar AM, Klibanov AL, Rychak JJ, Lindner JR, Ley K. Binding and detachment dynamics of microbubbles targeted to P-selectin under controlled shear flow. *J Control Release* 2004; 96:473–482.
25. Rychak JJ, Lindner JR, Ley K, Klibanov AL. Deformable gas-filled microbubbles targeted to P-selectin. *J Control Release* 2006; 114:288–299.
26. Weller GE, Villanueva FS, Klibanov AL, Wagner WR. Modulating targeted adhesion of an ultrasound contrast agent to dysfunctional endothelium. *Ann Biomed Eng* 2002; 30:1012–1019.
27. Weller GE, Villanueva FS, Tom EM, Wagner WR. Targeted ultrasound contrast agents: in vitro assessment of endothelial dysfunction and multi-targeting to ICAM-1 and sialyl Lewisx. *Biotechnol Bioeng* 2005; 92:780–788.
28. Wu Y, Unger EC, McCreery TP, et al. Binding and lysing of blood clots using MRX-408. *Invest Radiol* 1998; 33:880–885.

29. Alonso A, Della Martina A, Stroick M, et al. Molecular imaging of human thrombus with novel abciximab immunobubbles and ultrasound. *Stroke* 2007; 38:1508–1514.
30. Wheatley MA, Lathia JD, Oum KL. Polymeric ultrasound contrast agents targeted to integrins: importance of process methods and surface density of ligands. *Biomacromolecules* 2007; 8:516–522.
31. Cavalieri F, El Hamassi A, Chiessi E, Paradossi G, Villa R, Zaffaroni N. Tethering functional ligands onto shell of ultrasound active polymeric microbubbles. *Biomacromolecules* 2006; 7:604–611.
32. Ji J, Ji SY, He X, Ling WP. Preparation of ultrasound microbubbles crosslinked to albumin nanoparticles packaged with tissue-type plasminogen activator gene plasmid and method of in vivo transfection. *J Exp Pharmacol* 2011; 3:35–41.
33. Borrelli MJ. Methods for producing microbubbles. US patent 20110044903 A1. February 24, 2011.
34. Mullin LB, Phillips LC, Dayton PA. Nanoparticle delivery enhancement with acoustically activated microbubbles. *IEEE Trans Ultrason Ferroelectr Freq Control* 2013; 60:65–77.